ELSEVIER

Spectroscopic factors for the ^{9}Li ground state and $N = 6$ shell closure

R. Kanungo [a,b,*], A.N. Andreyev [b,c], L. Buchmann [b], B. Davids [b], G. Hackman [b], D. Howell [d],
P. Khalili [d], B. Mills [d], E. Padilla Rodal [b], Steven C. Pieper [e], J. Pearson [b], C. Ruiz [b], G. Ruprecht [b],
A. Shotter [b], I. Tanihata [b], C. Vockenhuber [b], P. Walden [b], R.B. Wiringa [e]

[a] Department of Astronomy and Physics, St. Mary's University, 923 Robie street, Halifax, NS B3H 3C3, Canada
[b] TRIUMF, 4004 Wesbrook Mall, Vancouver, BC V6T 2A3, Canada
[c] Department of Chemistry, Simon Fraser University, 8888 University Drive, Burnaby, BC V5A 1S6, Canada
[d] Department of Physics, Simon Fraser University, 8888 University Drive, Burnaby, BC V5A 1S6, Canada
[e] Physics Division, Argonne National Laboratory, 9700 S. Cass Avenue, Argonne, IL 60439, USA

Abstract

The ground state structure of ^{9}Li has been investigated through the $d(^9\text{Li}, t)^8$Li one-neutron transfer reaction at $E/A = 1.68$ MeV. The ^{8}Li sub-system in ^{9}Li was observed in its lowest three energy levels. The spectroscopic factors derived from a DWBA analysis are fairly consistent in trend with model calculations. The understanding of the $N = 6$ sub-shell closure from the spectroscopic information and neutron separation energies is discussed.

In recent years the appearance of new shell closures for neutron-rich nuclei has brought a new interest in our understanding nuclear orbitals and the nuclear effective interaction in these regions. The first evidence of breakdown of the conventional shell closure at $N = 20$ was pointed out through an enhancement in S_{2n} for Na isotopes [1]. This was later confirmed from B(E2) values measured by Coulomb excitation of neutron-rich Mg isotopes [2–6]. The $N = 8$ shell closure was also found to be dissolved for neutron-rich nuclei [7–9].

The disappearance of conventional shell closures however does not necessarily mean that shell structure is dissolved completely as one moves to neutron-rich or proton-rich regions. In parallel to disappearing conventional shell gaps, new shell gaps

have emerged in these regions. The first observation of a new shell closure at $N = 16$ neutron-rich nuclei was reported for O, N and F isotopes [10]. A more detailed discussion of the changes of shell closures in light neutron and proton-rich nuclei from separation energy systematics, beta decay Q-values and first excited states of even–even nuclei can be found in Refs. [11,12]. From these systematic studies, the possibility of a new sub-shell closure at $N = 6$ is suggested for neutron-rich isotopes [11]. This suggestion comes from the increased excitation energy of the first 2^+ state observed for the $N = 6$ He and Be isotopes. However, an increase in energy of the 2^+ state in even–even nuclei is not necessarily a confirmation of the existence of a shell gap, as discussed for example for $N = 40$ in Ref. [12]. One therefore needs detailed spectroscopy for a complete understanding.

A sub-shell closure at $N = 6$ was also suggested theoretically by Otsuka and collaborators [13]. The mechanism for the emergence of this sub-shell gap in their theoretical approach

was predicted to be the upward shift of the $1p_{1/2}$ orbital due to the spin–isospin interaction. A new semi-empirical mass formula also predicts a sub-shell closure at $N = 6$ [14].

In this Letter we report an investigation of the $N = 6$ sub-shell gap through the spectroscopic study of the ground state structure of ^{9}Li. In a ^{8}Li $+ n$ model, the ground state of ^{9}Li is a superposition of different configurations, in which the ^{8}Li 'core' is in different states. In the present experiment, the one-neutron transfer from ^{9}Li onto a deuteron target (i.e., the $d(^9\text{Li}, t)^8\text{Li}$ reaction) resulted in the ^{8}Li sub-system being observed in its different excited states. The spectroscopic factors derived for the different configurations show that the first three levels in ^{8}Li exhaust nearly half of the total occupation number in the p orbital. The evolution of sub-shell closure at $N = 6$ is discussed later based on spectroscopic strengths and neutron separation energies.

The experiment was performed using a ^{9}Li beam from the ISAC facility at TRIUMF, Canada, accelerated to 1.68 A MeV. The transverse beam emittance was 0.3 mm mrad/β and the beam spot on target had a diameter of 1 mm. The excellent beam properties enabled fairly good excitation energy resolution. A 100 μg/cm^2 deuterated polyethylene foil $(\text{CD}_2)_n$ served as the reaction target.

A schematic view of the experimental setup is shown in Fig. 1. The particles emitted in reactions of ^{9}Li with the target were detected using segmented annular silicon strip detector arrays. The LEDA array [15] (inner active radius $= 5$ cm and outer active radius $= 12.9$ cm) covered laboratory angles $\sim 25°–50°$. This annular array is physically separated into 8 identical sectors. Each sector has sixteen, 5 mm wide rings, that provide the information of the scattering angle. The LEDA array detected the tritons emitted from the $d(^9\text{Li}, t)^8\text{Li}$ reaction as well as deuterons emitted from $d(^9\text{Li}, d)^9\text{Li}$ elastic scattering.

The smaller array, S2, is a double-sided annular silicon strip detector. The front face is segmented in 48 rings, with 0.5 mm pitch. The reverse face is azimuthally segmented into 16 sectors. The heavy residues such as $^{9-7}$Li emitted in reactions with deuterons are detected by this array. In addition, ^{9}Li emitted in elastic scattering with the carbon component of the target were also detected. The S2 detector covered laboratory angles of $6°–17°$.
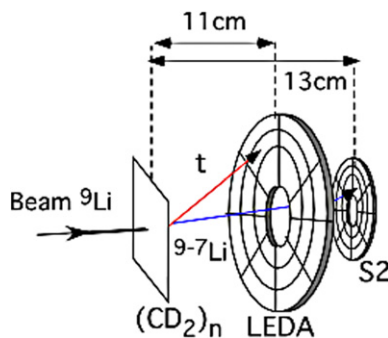
The kinematic curves observed in the S2 detector are shown in Fig. 2(a). The Rutherford scattering on carbon appears as the band nearly parallel to the angle axis, as labeled in the figure. This provides a measure of the beam intensity, which on an average was found to be $\sim 2 \times 10^5$/s. The beam intensity was therefore measured simultaneously with the transfer reaction throughout the experiment. This allowed us to minimize uncertainties due to beam intensity fluctuations while extracting the cross sections. The parabolic locus arises from $d + ^9$Li elastic scattering. The $d(^9\text{Li}, ^9\text{Li})d$ elastic scattering angular distribution plotted in the center-of-mass (cm) frame is shown in Fig. 2(b). The optical potential parameters for ^{9}Li $+ d$ interaction were derived from an optical model analysis of this angular distribution, as shown by the solid line in Fig. 2(b). The loci at higher energies than the elastic scattering (Fig. 2(a)) arise due to the one neutron transfer reaction $d(^9\text{Li}, ^8\text{Li}_{gs})t$ and $d(^9\text{Li}, ^8\text{Li}^*_{1+;0.98})t$ which have a positive Q-value. The angular region covered in the S2 detector for the transfer reaction of interest corresponds to the forward cm angle scattering $\sim 20°–40°$, referred to the reaction in normal kinematics, i.e., ^{9}Li(d, t). In this Letter, center-of-mass angle is the same as that for the reaction performed in normal kinematics. This definition is followed to retain the picture that an elastic scattering reaction is always peaked at forward center-of-mass angles.
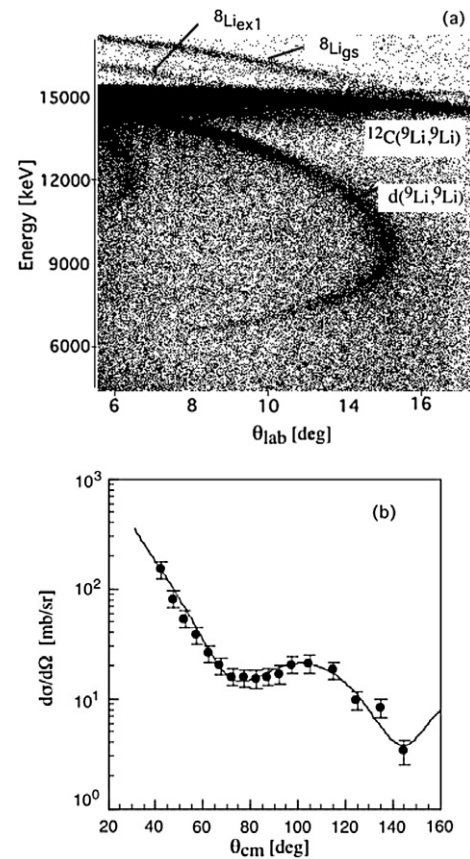

Fig. 2. (a) Laboratory energy vs scattering angle correlation for events in the S2 detector. (b) The elastic scattering ^{9}Li$(d, d)^9$Li angular distribution in the center-of-mass frame. The solid line shows the calculation with a phenomenological optical potential.

Fig. 1. Schematic view of experimental setup.

The loci for the light ejectiles observed in the LEDA array are shown in Fig. 3(a), (c). The deuterons from elastic scattering have the highest intensity as shown in the figure. The $d(^9\text{Li}, t)^8\text{Li}_{gs}$ and $d(^9\text{Li}, t)^8\text{Li}^*_{1+;0.98}$ loci appear above the elastic scattering band. The lower band below the $d(^9\text{Li}, d)$ was found to result from elastic scattering with protons, which indicated some hydrogen contamination in the target. The parabolic band is due to $d(^9\text{Li}, t)^8\text{Li}^*_{3+;2.25}$. This is more clearly visible when we observe the tritons in coincidence with the heavy residue in the S2 array as shown in Fig. 3(c). The angular coverage of the detectors did not cover coincident detection region for the $^8\text{Li}_{gs}$ and $^8\text{Li}_{ex1}$, therefore these loci do not appear in Fig. 3(c). The Q-value spectra are shown in Figs. 3(b) and (d) for the ^8Li states observed in Figs. 3(a) and (c) respectively.

The differential cross section for scattering in the center-of-mass frame was obtained from an analysis of the Q-value for the different states of ^8Li observed in the spectra described above. The background under the peaks was estimated using a linear fit. The angular distributions obtained are presented in Fig. 4. The error bars shown include both statistical and systematic errors. The beam intensity variation is taken into account in the statistical errors, as it was determined simultaneously with the transfer reaction throughout the experiment. The sys-

tematic errors include effects of target thickness (10%), coincidence efficiency (5%), solid angle (10%). The curves are finite range DWBA calculations using the code PTOLEMY [16]. The difference between the codes PTOLEMY and DWUCK5 [17] is the presence of core correction terms in PTOLEMY that improve the DWBA formalism. The effect of core correction is visible only at backward center-of-mass angles. Variational Monte Carlo (VMC) calculations were made for both the spectroscopic strength and radial shape of the d–t overlap (both s- and d-wave components) and the three ^8Li–^9Li overlaps [18,19]. Woods–Saxon potentials with wine-bottle modifications for use in the PTOLEMY entrance and exit channels were then constructed to reproduce these predicted radial shapes. These potentials correctly take into account the effective separation energies, i.e., $S_n(^9\text{Li}) + E^*(^8\text{Li})$. The total d–t spectroscopic factor in these calculations is 1.3 and the sum of the $p_{3/2}$ and $p_{1/2}$ factors for ^8Li–^9Li is shown in Table 2 and Fig. 5.

The $^9\text{Li} + d$ optical potentials were derived from fitting to the elastic scattering angular distribution in this work. To obtain the $^8\text{Li} + t$ potentials we started with the $^9\text{Be} + t$ potentials at 2.10 MeV [20]. The depth of the real part of the potential was then adjusted to suit the energy of this experiment and for ^8Li. This was done by linearly extrapolating the depths of $^8\text{Li} + p$ and $^8\text{Li} + d$ global optical potentials at the desired energy, to
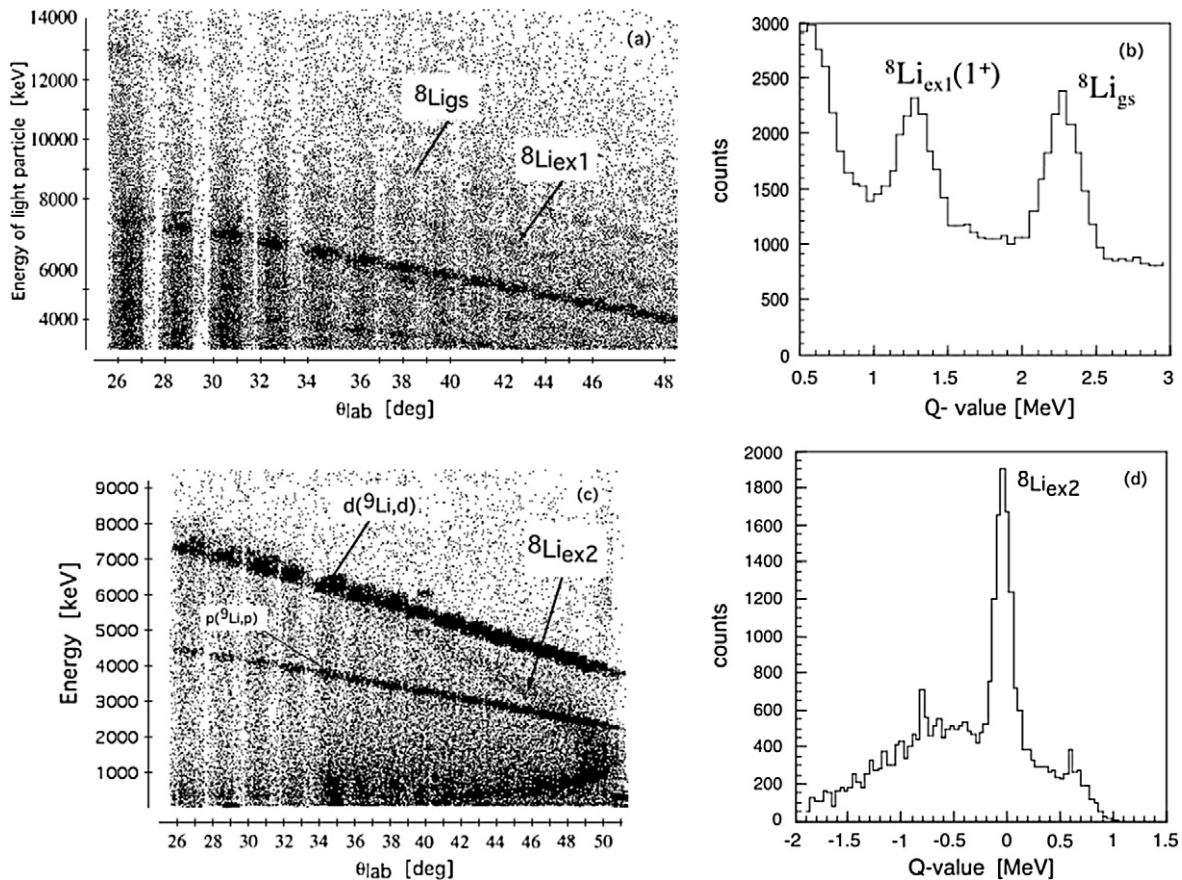

Fig. 3. Energy vs scattering angle correlations plots in the laboratory frame observed in the (a) LEDA array only, (c) LEDA array in coincidence with the S2 array. The Q-value spectrum for $d(^9\text{Li}, t)^8\text{Li}$ reaction for (b) the $^8\text{Li}_{gs}$ and $^8\text{Li}_{ex1}$ from LEDA only and (d) for the $^8\text{Li}_{ex2}$ from LEDA with S2 in coincidence. The effect of the elastic scattering curves in (c) has been omitted in the display of the Q-value plot in 3d. The vertical bands in (a) and (c) reflect the radial strips of the LEDA detectors.

^{8}Li + t. The depth of the ^{8}Li + d global optical potential was found to be in good agreement with that obtained from our measurement of ^{8}Li + d elastic scattering. The surface imaginary

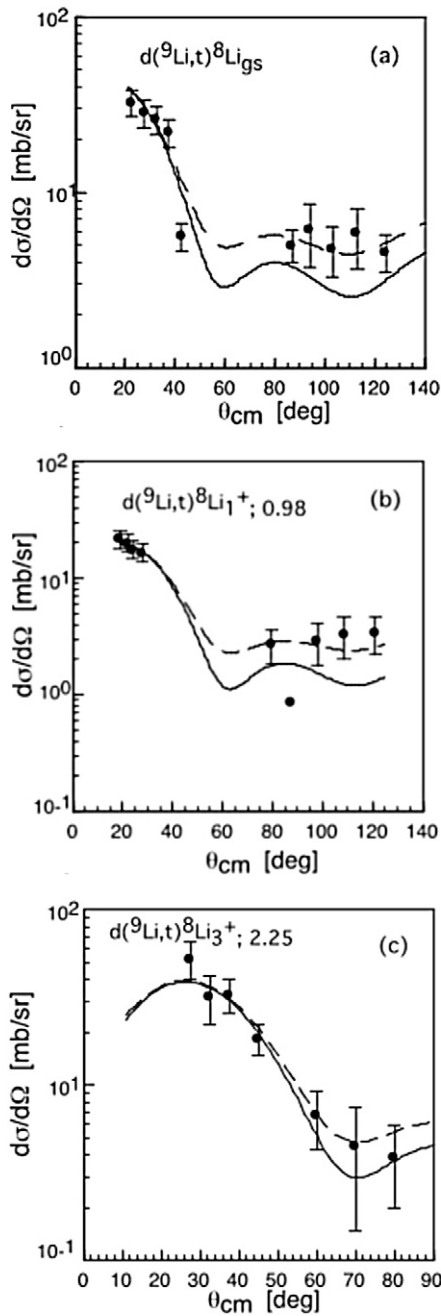Fig. 4. The differential cross section in the center-of-mass frame for (a) ^{8}Li$_{gs}$, (b) ^{8}Li first excited state, (c) ^{8}Li second excited state. The curves show DWBA calculations (*see text*). The center-of-mass angle shown here is that for the reaction viewed in normal kinematics, i.e., (d, t) reaction.

part was adopted from the ^{8}Li + d potential. It was decreased by the same percentage as the depth of the real part of the ^{8}Li + d potential was increased. The potentials used are listed in Table 1. Alternatively, we also considered the ^{7}Li + ^{3}He potential [21] for the exit channel. This slightly changes the normalization factor but the shape of the angular distribution in forward angles is unchanged. The effects of these two potential sets have been included in the uncertainties quoted for the spectroscopic factors.

The compound nuclear contribution to the differential cross section has a rather flat angular distribution [22,23], in contrast to the forward peaked nature of the experimental cross sections. The exact calculation for such an angular distribution is beyond the scope of this Letter. The noteworthy feature however is that the angular distribution at forward center-of-mass angles is therefore dominated by direct reaction mechanism. The spectroscopic information can thus be reliably determined from the forward center-of-mass angles. In this work we have therefore derived the spectroscopic factors from the data at forward center-of-mass angles only. The dashed curves in Fig. 4 show the DWBA angular distributions (with slightly smaller spectroscopic factors) added to the Compound Nuclear (CN) contributions used in Ref. [23]. At lower energies the compound nuclear effect is expected to be stronger. An upper limit of the effect could be considered as the cross section of the backward angle data in this experiment. The data in Fig. 4 agrees in magnitude with those in Ref. [23] for the ^{8}Li$_{1+;0.98}$ in the $\theta_{cm} = 80°$–$140°$ region, while it is 1.5 times smaller for the ^{8}Li$_{gs}$ in the same θ_{cm} region. The cross section for the ^{8}Li$_{3+;2.2}$ in the $\theta_{cm} = 60°$–$80°$ region agrees in magnitude.

A comparison of the spectroscopic factors obtained in this experiment to theoretical model predictions and other experiments is shown in Table 2. Comparison with different theories is shown in Fig. 5. The spectroscopic factors were obtained by normalizing the DWBA calculations with the VMC overlaps, to the respective angular distribution through a chi-square minimization. The spectroscopic factors are therefore the products of the VMC values and the renormalization factor. The resultant scaled angular distributions are shown in Fig. 4. The one standard deviation error bars for the spectroscopic factors include statistical and systematic fluctuations. The systematic fluctuations arise from the systematic error bars of the angular distribution (17%), the uncertainty in the exit channel optical potential (10%), and the difference in slope of the angular distribution for the ^{8}Li$_{gs}$ and ^{8}Li$_{ex1}$ compared to the DWBA calculations (10%). The systematic errors have been added in quadrature to the statistical ones. It is seen that the general trend of the spectroscopic factors are in fair agreement with the model calculations. It is seen that shell model predictions using a Cohen–Kurath (CK) interaction [24] (filled circles) agree well

Table 1
Optical potential parameters

Channel	V_0 [MeV]	r_0 [fm]	a_0 [fm]	W_s [MeV]	r_s [fm]	a_s [fm]	W_v [MeV]	r_v [fm]	a_v [fm]	V_{so} [MeV]	r_{so} [fm]	a_{so} [fm]
^{9}Li + d	67.5	1.54	0.68	3.1	1.72	0.4						
^{8}Li + t	125	0.8	0.7	3.3	2.06	0.66	2.91	2.06	0.72	8.93	1.07	0.66

for the $^8\text{Li}_{ex1}$ while the deviation increases for $^8\text{Li}_{gs}$ and $^8\text{Li}_{ex2}$. The Variational Monte Carlo (VMC) calculations (filled triangles) predict spectroscopic factors that are in good agreement with $^8\text{Li}_{ex2}$ while they are higher than the experimental observations for the ground state and first excited state of ^8Li. The CK shell model, the VMC calculations and the experimental observations all agree on the ordering of spectroscopic strength (Fig. 5). The No Core Shell Model (NCSM) [25] agrees well (open circle) with the VMC for $^8\text{Li}_{gs}$. The second line of Table 2 shows the spectroscopic factors extracted from using the compound nuclear contributions from Ref. [23]. If our backward angle cross section is taken as the upper limit of the compound nuclear contribution, it will result in a 5–10% decrease of spectroscopic factors.

The spectroscopic factors for the $^8\text{Li}_{gs}$, $^8\text{Li}_{ex1}$ and $^8\text{Li}_{ex2}$ have a large deviation from those reported in Ref. [23]. The reason for this is not well understood. There are some differences between the present data and that of Ref. [23]. In this work we determine the spectroscopic factors exclusively from the forward center-of-mass angle scattering data. In contrast, those in Ref. [23] are determined only from the larger center-of-mass angles. The incident beam intensity was measured by Rutherford scattering in this work, while that in Ref. [23] was deduced with help of optical model analysis. Therefore, some ambiguity in normalization may exist in Ref. [23]. Apart from these, ambiguities in optical potentials could also contribute to the differences in the spectroscopic factors. The spectroscopic

factor for the $^8\text{Li}_{gs}$ derived in this work is smaller (Table 2) than that obtained from $^8\text{Li}(d, p)^9\text{Li}_{gs}$ reaction at $E/A = 9.5$ MeV in Ref. [26], but in agreement with the $E/A = 4.9$ MeV result of the same reaction in Ref. [27]. It is also in agreement with that obtained from $^9\text{Be}(^8\text{Li}, ^9\text{Li})$ reaction in Ref. [28].

The total spectroscopic factor of neutrons occupying the p-orbital obtained from this experiment is 1.81 ± 0.43. The model calculations indicate that 95% of the total strength is from the $p_{3/2}$ orbital. In comparison, the $^{11}\text{B}(d, t)^{10}\text{B}$ reaction yields a total spectroscopic factor of 4.17 for the three lowest 3^+, 1^+ and 0^+ levels of ^{10}B [29]. The spectroscopic factor for $^{12}\text{C}(p, d)^{11}\text{C}_{gs}$ is also found to be 4.0 [30]. The $^9\text{Be}(d, p)^{10}\text{Be}$ on the other hand shows a spectroscopic factor of 1.67 ± 0.69 for the $p_{3/2}$ neutrons [22]. These seem to suggest that the sub-shell gap at $N = 6$ is larger for ^{12}C and ^{11}B as compared to ^{10}Be and ^9Li.

A measure of the gap between the $p_{3/2}$ and the next orbital can be obtained by the difference in one neutron separation energy (S_n) of the $N = 5$ and $N = 7$ isotopes. This gives us an estimate of the $N = 6$ shell gap for each element. Similarly the difference in S_n between the $N = 7$ and $N = 9$ isotopes provides a measure of the gap of $N = 8$. Fig. 6 shows this systematic study for lithium to fluorine isotopes using the masses
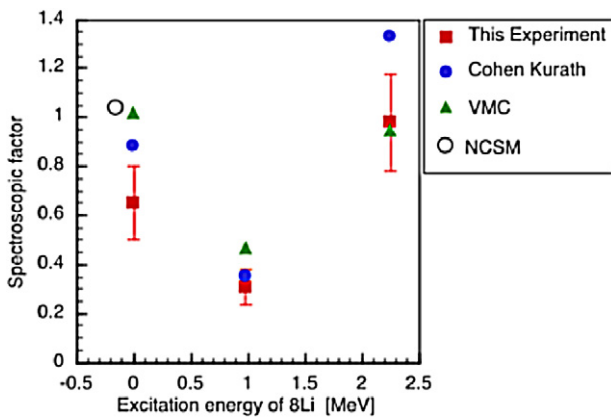

Fig. 5. Comparison of theoretical spectroscopic factors to those obtained in this experiment for $d(^9\text{Li}, t)^8\text{Li}$. *See index and text for details.*
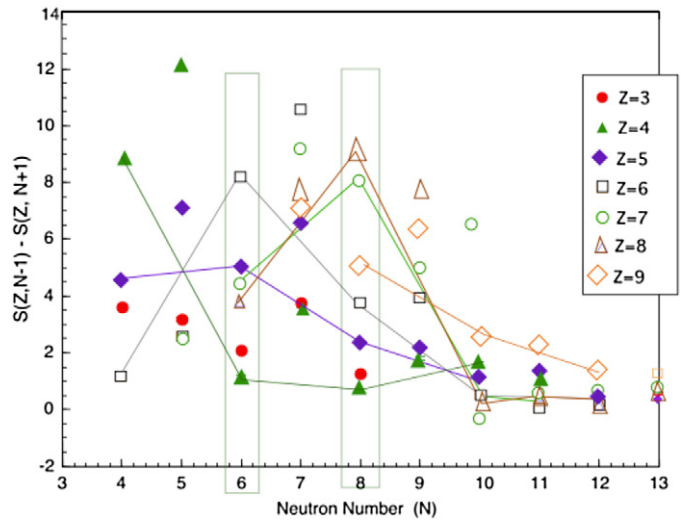

Fig. 6. Systematic trends of $S_n(Z, N - 1) - S_n(Z, N + 1)$ for different isotopic chains as indexed in the figure. The lines join the even N isotopes to guide the eye.

Table 2
Spectroscopic factors

Reaction	$^9\text{Li} = {}^8\text{Li}_{gs} + n$	$^9\text{Li} = {}^8\text{Li}_{0.98} + n$	$^9\text{Li} = {}^8\text{Li}_{2.25} + n$	Reference
$d(^9\text{Li}, t)$	0.65 ± 0.15	0.31 ± 0.07	0.98 ± 0.2	This work (no CN)
$d(^9\text{Li}, t)$	0.59 ± 0.15	0.28 ± 0.07	0.94 ± 0.2	This work (with CN)
$d(^9\text{Li}, t)$	1.95 ± 0.14	0.82 ± 0.17	2.4 ± 0.27	[23] T1
$d(^8\text{Li}, p)$	0.90 ± 0.13			[26]
$d(^8\text{Li}, p)$	0.68 ± 0.14			[27]
$^9\text{Be}(^8\text{Li}, ^9\text{Li})$	0.62 ± 0.13			[28]
VMC (theory)	1.02 ± 0.08	0.47 ± 0.04	0.95 ± 0.07	[18,19]
CK (theory)	0.88	0.36	1.33	[24]
NCSM	1.05			[25]

from Ref. [31]. It should be mentioned however, that the quantity $[S_n(Z, N-1) - S_n(Z, N+1)]$ may not give the absolute value of shell gaps if other structure effects are present. The interesting point here is the relative behaviour of the gap for the different isotopic chains. The large gap of $N = 6$ observed for the carbon chain at ^{11}C could be partly an effect of the alpha cluster structure of ^{12}C. It is interesting to note that the behaviour of the shell gap for $Z = 3$ to $Z = 6$ as seen in Fig. 6 is consistent with the trend of the total spectroscopic factors for these isotopes.

The weakening of the $N = 8$ shell gap for low Z isotopes is also seen in Fig. 6. This study therefore reveals that for very neutron-rich nuclei since the $N = 8$ shell gap disappears, the gap at $N = 6$ seems to become more prominent in manifesting itself as a shell closure-like behaviour in these regions. It is probably because of this reason that we observe the smallest charge radius of the lithium isotopes at ^{9}Li [32], showing it to have much less deformation. The increased two-neutron separation energy and excitation energy of ^{8}He as compared to ^{6}He is also consistent with a shell-gap like behaviour at $N = 6$.

In summary, the subsystem ^{8}Li (core) inside ^{9}Li was found to reside in its ground state and both bound as well as unbound excited states. This was ascertained through a one neutron transfer $d(^9\text{Li}, t)^8\text{Li}$. The total spectroscopic factor for the overlap of ^{9}Li with a neutron and ^{8}Li in its first three states is 1.81 ± 0.43. Both traditional shell model and current VMC calculations indicate that 95% of this strength is in the $p_{3/2}$ orbital. A comparison of the spectroscopic amplitudes and the neutron separation energies for the different isotopic chains suggest that the gap at $N = 6$ is larger for $Z = 5$ and 6 than $Z = 3$ and 4. However the $N = 8$ gap becomes very weak, disappearing for the low Z isotopes, allowing the $N = 6$ sub-shell gap to show its dominance in these regions.

Acknowledgements

References

[1] C. Thibault, et al., Phys. Rev. C 12 (1975) 644.
[2] D. Guillemaud-Mueller, et al., Nucl. Phys. A 426 (1984) 37.
[3] T. Motobayashi, et al., Phys. Lett. B 346 (1995) 9.
[4] B.V. Pritychenko, et al., Phys. Lett. B 461 (1999) 322.
[5] J.A. Church, et al., Phys. Rev. C 72 (2005) 054320.
[6] D. Lunney, et al., Eur. Phys. J. A 28 (2006) 129.
[7] H. Iwasaki, et al., Phys. Lett. B 491 (2000) 8.
[8] A. Navin, et al., Phys. Rev. Lett. 85 (2000) 266.
[9] I. Tanihata, R. Kanungo, C. R. Physique 4 (2003) 437.
[10] A. Ozawa, et al., Phys. Rev. Lett. 84 (2000) 5493.
[11] R. Kanungo, et al., Phys. Lett. B 528 (2002) 58.
[12] R. Kanungo, Phys. Lett. B 649 (2007) 31.
[13] T. Otsuka, et al., Phys. Rev. Lett. 87 (2002) 082502.
[14] C. Samanta, S. Adhikari, Phys. Rev. C 65 (2002) 037301.
[15] T. Davinson, et al., Nucl. Instrum. Methods A 454 (2000) 350.
[16] M.H. Macfarlane, S.C. Pieper, Argonne National Laboratory Report No. ANL-76-11, Rev. 1, 1978.
[17] P. Kunz, unpublished.
[18] R.B. Wiringa, et al., Phys. Rev. C 62 (2000) 014001.
[19] S.C. Pieper, K. Varga, R.B. Wiringa, Phys. Rev. C 66 (2002) 044310.
[20] L. Cohen, G.H. Herling, Nucl. Phys. A 141 (1970) 595.
[21] R.L. Dixon, R.D. Edge, Nucl. Phys. A 156 (1970) 33.
[22] A. Szczurek, et al., Z. Phys. A 333 (1989) 271 and references therein.
[23] H.B. Jeppesen, et al., Phys. Lett. B 635 (2006) 17.
[24] S. Cohen, D. Kurath, Nucl. Phys. A 101 (1967) 1.
[25] P. Navratil, Phys. Rev. C 70 (2004) 054324.
[26] A.H. Wuosmaa, et al., Phys. Rev. Lett. 94 (2005) 082502.
[27] Z.H. Li, et al., Phys. Rev. C 71 (2005) 052801(R).
[28] V. Guimarães, et al., Phys. Rev. C 75 (2007) 054602.
[29] W. Fitz, et al., Nucl. Phys. A 101 (1967) 449.
[30] H. Ohnuma, et al., Phys. Lett. B 147 (1984) 253.
[31] G. Audi, et al., Nucl. Phys. A 729 (2003) 337.
[32] R. Sanchez, et al., Phys. Rev. Lett. 96 (2006) 033002.